# CLOUD-RADIATION EXPERIMENTS CONDUCTED WITH GLAS GENERAL CIRCULATION MODELS

by

Gerald F. Herman

Department of Meteorology
University of Wisconsin, Madison, WI 53706
and
Laboratory for Atmospheric Sciences
NASA Goddard Space Flight Center, Greenbelt, MD 20771

ABSTRACT

The cloud and radiation budget climatologies of GLAS second order general circulation models are assessed for the January-February and July periods, and the models' radiation and cloud parameterizations are briefly reviewed. Systematic errors in the computed infrared radiation budget are attributed to difficulties in treating the infrared optical properties of clouds, and in predicting subgrid scale fractional cloudiness. The solar radiation balance is generally reasonable, although some discrepancies with observations occur during the Southern Hemisphere summer. Problems with the models' cloud climatology include excessive low cloudiness during the Northern Hemisphere winter, and a failure to simulate adequately the advance and retreat of the ITCZ.

Four cloud feedback experiments that were conducted with GLAS GCMs are reviewed. These include transparent cloud experiments, fixed and variable cloud experiments, and desert albedo feedback experiments. The role of radiation in the maintenance of the Siberian high also is investigated.

## 1. INTRODUCTION

The general circulation models (GCMs) of NASA's Goddard Laboratory for Atmospheric Science (GLAS) have been widely applied to problems of weather forecasting, and in climate sensitivity and simulation studies. A striking and sometimes disturbing conclusion that frequently emerges from the analyses of these GCM calculations is that the results are sensitive to a significant degree either to the parameterizations of solar or infrared radiation, or to the computational procedure through which the radiative fluxes interact with clouds, the gaseous atmosphere, or the surface of the earth. In most cases, the nature of the sensitivity is complicated, and frequently is ascribed to processes that are loosely termed cloud-radiative interactions or cloud-radiative feedback.

There are two broad problems involving the relationship between clouds and radiation that arise in the numerical modeling of weather and climate. There is always an interaction between clouds and radiation insofar as when a stream of radiation encounters cloud particles, there is either a redirection of energy from the incident stream (scattering), or an exchange of energy between the radiation field and the thermal energy of the cloud particles (absorption or emission). These interactions between clouds and radiation essentially determine the amount of radiative energy that is available to the earth-atmosphere system. Thus, the influence or effect of clouds on the radiation must be properly represented in numerical simulations of climate or the general circulation, and this is accomplished by specifying the optical properties of the atmosphere and of the earth's surface. The optical properties may themselves depend on the disposition of the radiation, as in the case of when radiative cooling induces cloud formation. The mutual adjustment of the cloud and radiation fields to a state that is consistent with the internal dynamics of a model is termed cloud-radiative feedback. A fundamental and essentially unanswered question has been whether the detailed simulation of cloud-radiative feedback is critical for climate and general circulation sensitivity studies. Likewise, neither the importance of cloud influences nor the effect of cloud-radiative feedback have been established for short- and medium-range forecasting efforts.

We summarize here the principal features of the cloud and radiation budget climatologies of GLAS GCMs. These fields are compared with observed climatologies to assess the reliability of model-generated fields, and to illustrate potential cloud influences on the radiative balance of the model. Also discussed are several GCM experiments conducted at GLAS in which the results clearly were dependent on the nature of the cloud interactions with the model radiation and dynamics. These latter discussions involving potentially complicated cloud feedbacks are at the same time qualitative, speculative, and perhaps model dependent. They also illustrate the inherent difficulty that exists in attempting to deduce the nature of cloud-radiative feedbacks based on the output generated by a global circulation model.

## 2. CLOUD PARAMETERIZATION AND RADIATIVE TRANSFER

Many details of the GLAS GCMs have been described by Somerville et al. (1974), Stone et al. (1977), and Halem et al. (1979). Here it suffices to note that the GLAS model is a nine-layer primitive equation model utilizing a $\sigma$-vertical coordinate formulation together with a 4° latitude by 5° longitude horizontal grid. Ocean surface temperatures and polar sea ice boundaries are prescribed to vary according to a pre-determined climatology, while ground temperatures over land and ice are calculated from the surface energy balance. Simple approximations are used for ground moisture conditions, and surface fluxes of heat and moisture are based on drag laws that account for the stability and windshear in the boundary layer, and the roughness of the surface.

Cloud formation processes in the model are fully coupled to cloud radiative processes insofar as clouds grow and dissipate in response to changes in temperature, stability, and surface heating, and these depend in part on the flux and flux divergence of solar and thermal radiation. The parameterization of these cloud and radiative processes are described below.

Convective cloud formation in the GLAS model (see Helfand, 1979) follows the Arakawa three level cumulus cloud parameterization. Convection occurs if air at a cloud base layer becomes buoyant during its moist adiabatic ascent to the cloud top layer.

Convective clouds (see Fig 1) are said to be penetrative when the lowest 6 model layers participate in the vertical mixing; while low-level convection involves σ-layers 7 and 8, and upper-level convection involves layers 5 and 6. Supersaturation clouds in the model, which represent stratiform clouds in nature, form simply when the water vapor mixing ratio at a grid point exceeds the saturation mixing ratio for the ambient temperature.

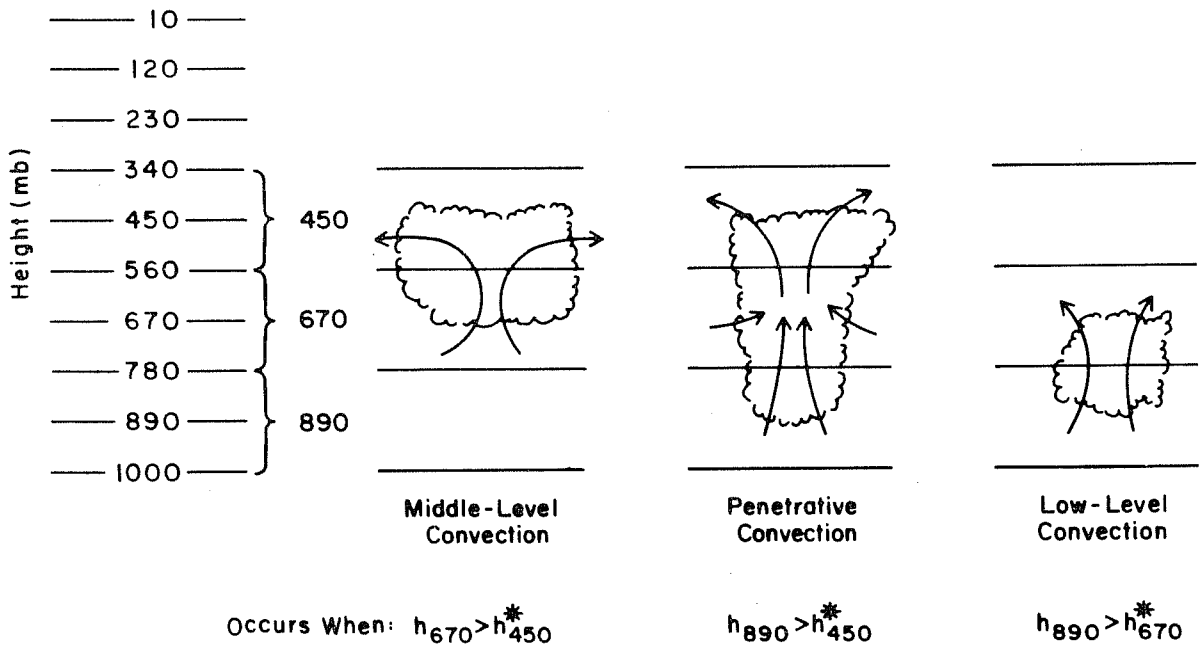


Figure 1. Convective cloud formation with the 3-layer "strapped" Arakawa scheme. (after Helfand, 1979).

Solar radiation in the GLAS model has been computed using the formulation of Lacis and Hansen (1974). Ozone absorption is treated with accurate empirical formulae based on detailed multiple scattering calculations and laboratory measurements of ozone absorption. Water vapor absorption under clear-sky conditions is computed with the Yamamoto (1962) data, and under cloudy conditions this absorption is reformulated with a "k-distribution" for use in conjunction with a two-stream approximation. In the published version of the Lacis

and Hansen parameterization neither absorption by the liquid water droplets nor the solar zenith angle dependency of clouds or of the surface is represented. Modifications to the GLAS solar radiation code have been made by Davies (1980) to include the effect of solar elevation on the surface albedo, and to introduce solar zenith angle angle dependency into the cloud multiple scattering calculations with a δ-Eddington two-stream approach. The preliminary results indicate that the effects of these modifications are substantial, e.g., when the new zenith angle dependency was introduced into test runs the planetary albedo of the model increased from 31 to 37%.

In the present version of the GLAS radiation code the optical properties of the cloud (i.e., optical depth and single scatter albedo) are prescribed quantities, since cloud liquid water is not a predicted model variable at the present time. Thus, cloud optical thickness depends only on cloud type, and the vertical layer in which the cloud forms. (see Table 1)

The calculation of solar radiation requires approximately 2 seconds of CPU time to compute the entire 46x72 array of vertical profiles at each time step. This represents approximately 10% of the time required for the total GCM calculation at time steps when the solar radiation routine is called. At present it is called every third time step, or every 30 minutes.

Table 1. Prescribed cloud properties in GLAS solar radiation calculations.

| Cloud origin | Cloud type | Albedo (%) | Optical Thickness |
|---|---|---|---|
| Convective | | | |
| mid-level | Ac | 50 | 8 |
| low-level | Cu | 70 | 16 |
| penetrating | Cb | 80 | 32 |
| | | | |
| Supersaturation | | | |
| 0-400 mb | Ci | 20 | 2 |
| 400-700 mb | As | 50 | 8 |
| 700-1000 mb | St | 70 | 16 |

Infrared radiation in the GLAS GCM originally was computed according to an algorithm developed by J. Hogan and described in Somerville et al. (1974). In recent years the Hogan calculation was replaced by the more detailed code developed by Wu and Kaplan (see Wu, 1980). A significant price was paid for this increased accuracy: The running time of the Hogan version of the code was about 40 seconds. For the same calculations the Wu-Kaplan algorithm required 150-200 seconds per call to the longwave radiation.

The Wu calculation closely follows the formulation of Rodgers and and Walshaw (1966), although revised spectral data are used in the 6.3 μm water vapor band and in the continuum region. Ozone and carbon dioxide transmission are parameterized on the basis of precomputed line by line calculations. All clouds in the infrared calculation are assumed to be optically thick.

Significant differences in the GLAS model climatology occurred when the Hogan calculation was replaced with the Wu-Kaplan routine. (see Wu et al., 1978). In general the differences between cooling rates computed by the Wu-Kaplan and Hogan algorithms were small in the mid-troposphere, but cooling rates in the upper troposhere and lower stratosphere were larger with the Wu-Kaplan formulation because of its improved treatment of $CO_2$ absorption. Cooling rates were also larger in the lower troposhere at low latitudes because of the inclusion of water vapor dimer absorption.

## 3. RADIATION CLIMATOLOGY OF THE GLAS GCM.

In general, the realistic simulation of the radiation budget of the earth-atmosphere system may be viewed as a necessary, but not sufficient, condition for concluding that a model can accurately simulate the observed climate. If the GCM's radiation balance agrees with observations, it is one of several indications that the dynamical processes which determine the distribution of cloudiness, water vapor, and temperture are properly simulated. By itself, a correct radiation balance does not ensure that the simulated general circulation is correct or even reasonable.

The model's radiation balance that is discussed here may be viewed as a model climatology insofar as it is based on ensemble averages computed from a number of January-February and July simulations. The January-February simulations to which we refer were derived from the runs used in the ice margin experiments of Herman and Johnson (1978) and in the sea surface temperature anomaly experiments of Shukla and Bangaru (1975). These simulations were initialized with 00 GMT 1 January conditions, and averages were obtained from model data sampled at 12 hour intervals during the last 30 days of the 45 day simulations. Thus, the monthly averages refer to the mean defined over the time interval 1200 GMT 15 January to 1200 GMT 14 February. The July simulations were obtained from the climate variability and predictability studies conducted at GLAS by Dr. J. Shukla and collaborators. They were initialized with 00 GMT 15 June NMC conditions, or perturbations thereof, and averages were computed from data collected at 12 hour intervals between 1 July and 1 August. The model climatology was thus formed from the respective averages of the eight January-February simulations and seven July simulations. More details of the individual runs used in the climatology appear in Herman and Johnson (1980, Table 1). It is assumed that the GCM data that are sampled after fifteen days of integration are sufficiently independent of the initial conditions, and thus the fields are representative of the GCM's internal adjustment to the boundary conditions and external forcing.

The model's radiation climatology is compared in Figures 2 and 3 with the observed satellite-derived radiation climatology recently compiled by Winston et al. (1979) for the for the January-February and July periods.

The most striking feature of the model's infrared radiation budget at the top of the atmosphere is the large and systematic underestimation of the amount of radiation lost to space during both seasons. On the average this systematic bias is 30-40 $Wm^{-2}$, but becomes as large as 60-70 $Wm^{-2}$ during the winter in the high latitudes of the Northern Hemisphere.

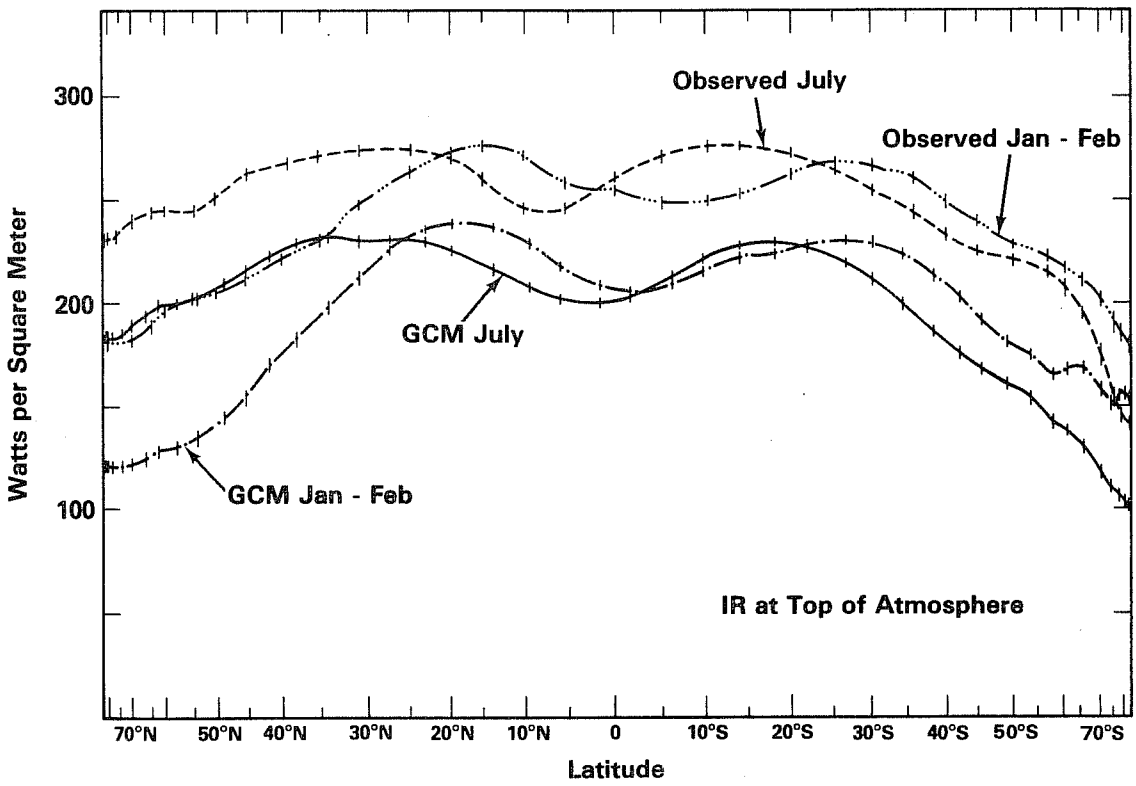


Figure 2. Observed and simulated net longwave radiation at the top of the atmosphere. Key: Simulated July _____ ; Observed July _ _ _; Simulated January-February____ _ ___ _; Observed January-February ___ _ _ _ ____ _ _ _;

The reason that the model fails to emit enough thermal radiation to space is due to its difficulties in properly representing the infrared optical properties of model-generated clouds. Firstly, all clouds in the model are treated as being completely opaque (i.e., having unit emissivity) irrespective of their temperature. Thus the model does not distinguish between liquid water and ice clouds, and does not account for the semi-transparent properties of cirrus, or thin stratiform clouds. It is commonly accepted that these latter cloud types have emissivities that depart substantially from unity, and are thus capable of transmitting to space warmer radiation that is emitted from the surface or lower troposphere.

Secondly, all model clouds, including those that result from subgrid scale cumulus convection, are assumed to occupy the entire (~400x400km$^2$) grid area. Hence fractional cloudiness is not represented, and model clouds at each grid point trap more radiation than do the scattered and broken cloud fields that occur in nature.

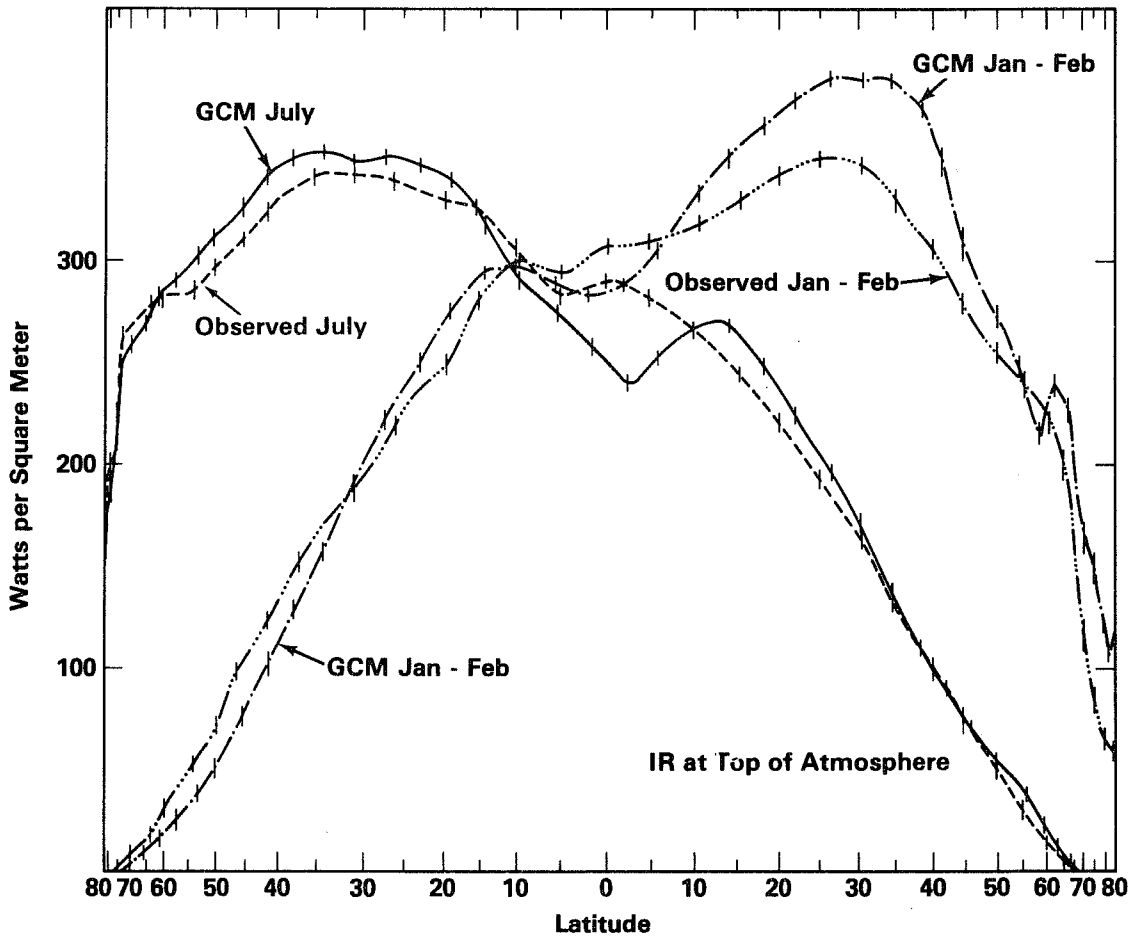


Figure 3. Observed and simulated solar radiation absorbed by the earth atmosphere system. Key is the same as in Fig 2.

Modifications to the Wu-Kaplan radiation scheme recently have been made to account for both fractional cloudiness and variable emissivity (see Herman and Krishnamurthy, 1981), although extended integrations have not yet been carried out. Vertical profiles of the flux and flux divergence calculated for different cloud fractions and emissivities are shown in Table 2. It is clear that specifying the proper cloud fraction and emissivity potentially provides the means for bringing the model longwave radiation balance into closer agreement with the observations. Clearly, the difficult theoretical problem here lies in parameterizing the fractional sub-grid distribution of cloudiness based on the internal dynamics and thermodynamics of the model.

Table 2. Longwave fluxes and cooding rates for various cloud fractions (f) and cloud transmissivity ($T_c$). Values are for clouds in sigma-layer 5, 46° N, for 1 February. (Details of calculation appear in Herman and Krishnamurthy, 1981.)

| Level | Pressure (mb) | Flux(W $m^{-2}$) | | | | |
|---|---|---|---|---|---|---|
| | | Cloudless $f=0.0, \bar{T}_c=1.0$ | $f=0.25, \bar{T}_c=0.0$ or $f=1.0, \bar{T}_c=0.75$ | $f=0.5, \bar{T}_c=0.0$ or $f=1.0, \bar{T}_c=0.5$ | $f=0.75, \bar{T}_c=0.0$ or $f_c=1.0, \bar{T}_c=0.25$ | $f=1.0$ $\bar{T}_c=0.0$ |
| 1 | 10 | 211 | 195 | 179 | 164 | 148 |
| 2 | 120 | 205 | 189 | 173 | 157 | 141 |
| 3 | 230 | 197 | 181 | 164 | 148 | 131 |
| 4 | 340 | 187 | 170 | 153 | 136 | 119 |
| 5 | 450 | 170 | 152 | 134 | 116 | 98 |
| 6 | 560 | 151 | 126 | 100 | 75 | 49 |
| 7 | 670 | 134 | 113 | 92 | 72 | 51 |
| 8 | 780 | 118 | 101 | 83 | 66 | 48 |
| 9 | 890 | 104 | 89 | 74 | 59 | 44 |
| 10 | 1000 | 90 | 77 | 64 | 51 | 39 |

| Layer | Pressure at Center of Layer (mb) | Cooling Rate (°C/Day) | | | | |
|---|---|---|---|---|---|---|
| | | Cloudless $f=0.0, \bar{T}_c=1.0$ | $f=0.25, \bar{T}_c=0.0$ or $f=1.0, \bar{T}_c=0.75$ | $f=0.5, \bar{T}_c=0.0$ or $f=1.0, \bar{T}_c=0.5$ | $f=0.75, \bar{T}_c=0.0$ or $f=1.0, \bar{T}_c=0.25$ | $f=1.0$ $\bar{T}_c=0.0$ |
| 1 | 65 | 0.4 | 0.5 | 0.5 | 0.5 | 0.6 |
| 2 | 175 | 0.6 | 0.6 | 0.7 | 0.7 | 0.7 |
| 3 | 285 | 0.8 | 0.9 | 0.9 | 0.9 | 0.9 |
| 4 | 395 | 1.3 | 1.4 | 1.4 | 1.5 | 1.6 |
| 5 | 505 | 1.4 | 2.0 | 2.6 | 3.2 | 3.8 |
| 6 | 615 | 1.3 | 1.0 | 0.6 | 0.2 | -0.2 |
| 7 | 725 | 1.2 | 1.0 | 0.7 | 0.5 | 0.2 |
| 8 | 835 | 1.1 | 0.9 | 0.7 | 0.5 | 0.3 |
| 9 | 945 | 1.1 | 0.9 | 0.8 | 0.6 | 0.4 |

In general the solar radiation absorbed by the model's earth-atmosphere system agrees well with the observations, except in the mid-latitudes of the Southern Hemisphere during July and in the equatorial regions during January. It is plausible that this excess absorption in the Southern Hemisphere is a consequence of the relatively small values of cloudiness (and lower planetary albedo) simulated during January between 10° and 40°S. However, the cloudiness is also underestimated during the Northern Hemisphere summer, but the differences between the observations and the simulations are not as large as in winter.

## 4. CLOUD CLIMATOLOGY OF THE MODEL.

The cloud climatology of the GLAS GCM was obtained from the eight January-February and seven July simulations described in Section 3. As a measure of cloudiness in the model we use cloud frequency, which is defined as the fraction of the total integration time during which a specified cloud type occurred at a grid point.

The zonally-averaged model cloud frequency is illustrated in Figure 4a and 4b. For comparison we also illustrate the zonal values for January and July tabulated by Berlyand and Strokina (1975), and also values interpolated from the zonal summary presented by Gates and Schlesinger, (1977). Of course, only a qualitative comparison is possible because of the disparity between the definitions of "cloudness" used in the different sources. The Beryland and Strokina and Gates and Schlesinger data are mixtures of surface and satellite observations, and are supplemented by inferences from other analyses. The precise relationship between the measures of cloudiness reported in these analyses and the cloud frequency in the GCM is yet unclear. The gross features of the global climatology are simulated by the model: Maximum cloudiness occurs in mid-and high latitude, and in the equatorial tropics, with minimum cloudiness in the subtropical regions.

The southward shift of the tropical maximum from July to January corresponding to the southward migration of the ITCZ is apparent in the Berlyand and Strokina data, and is simulated by the GCM. However, the amplitude of the simulated shift is extremely small as compared with observations. In the high latitudes of the northern

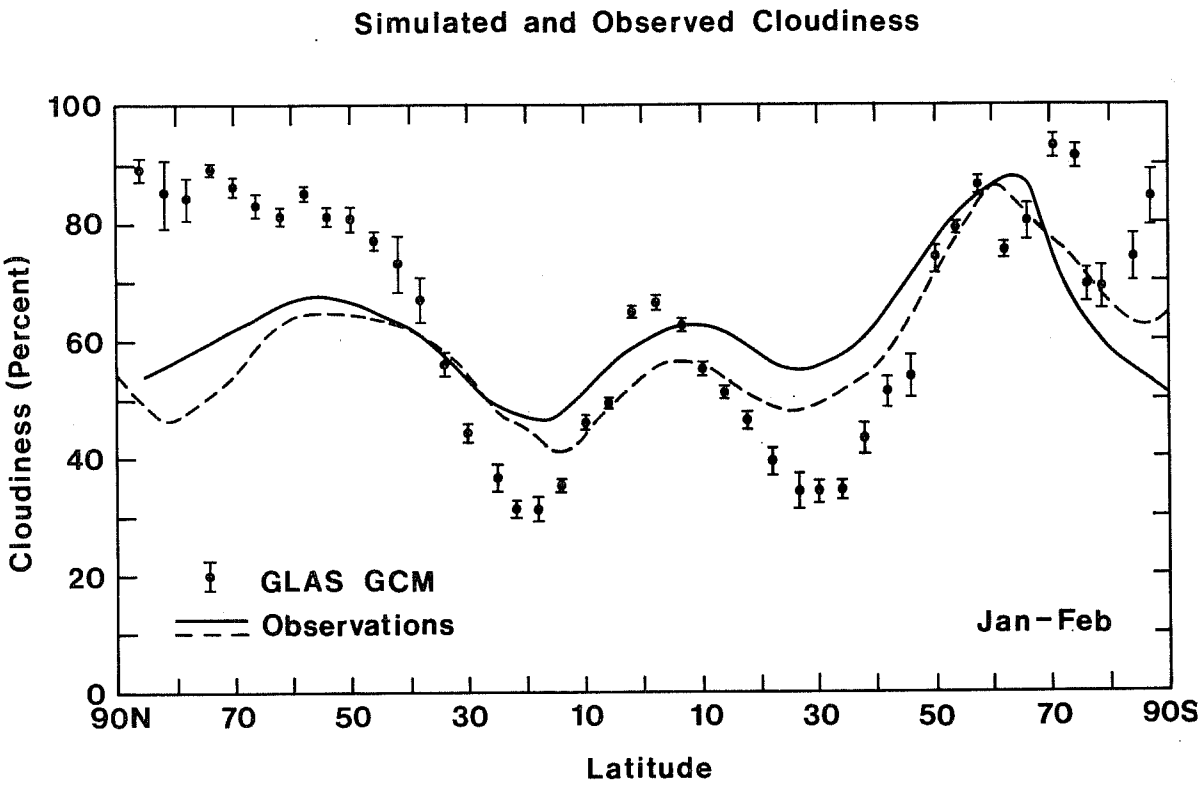


Figure 4a. Observed zonal cloudiness from Berlyand and Strokina (solid line) and as compiled by Gates and Schlesinger (1977). Bars indicate the inherent variability of model-generated cloudiness.

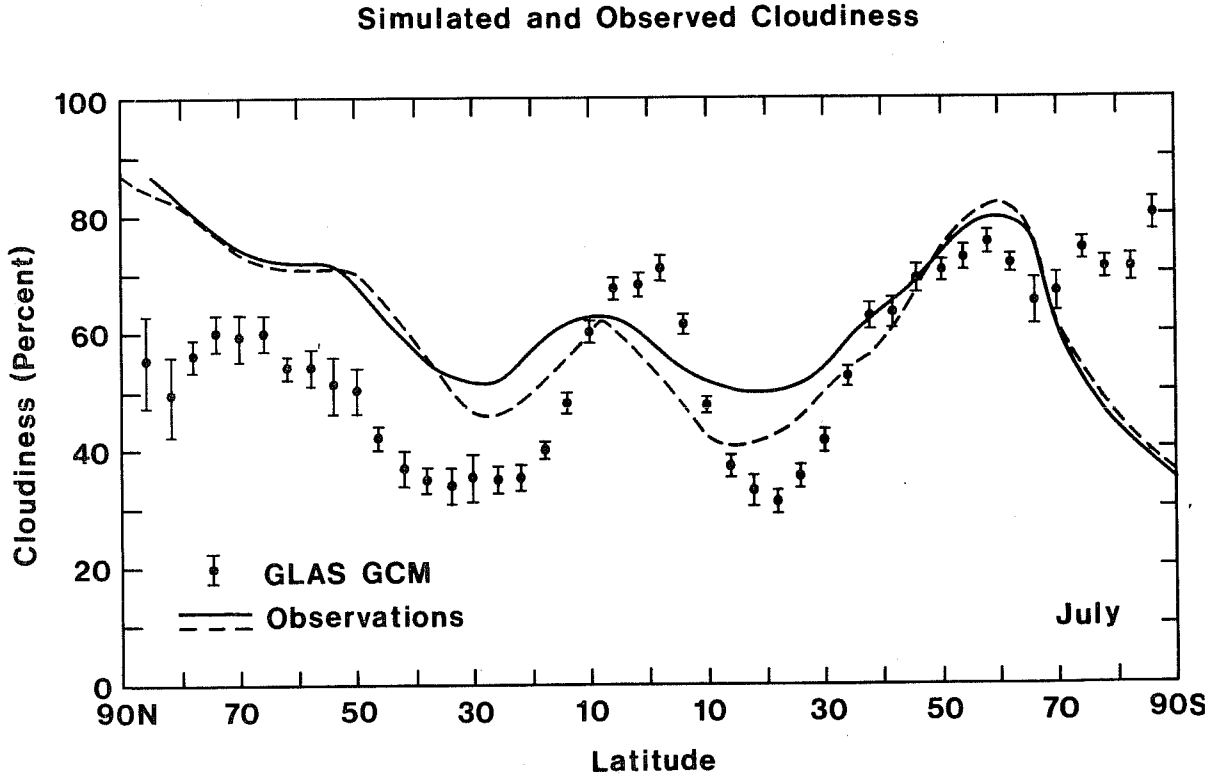


Figure 4b. As in Figure 4a, except for July.

hemisphere (north of 60°N) the observations show that maximum cloud cover occurs during the summer, due primarily to the buildup of stratus over the Arctic Basin and convective cloudiness over the adjacent continents. The cloudiness diminishes in winter owing to the development of the relatively cloudfree continental anticyclones. This trend is reversed in the GCM due to the wintertime buildup of stratiform clouds throughout the high mid-latitudes of the northern hemisphere. Elsewhere a detailed comparison is difficult to obtain.

The observed global distribution of cloudiness obtained by Berlyand and Strokina (1980) is shown in Figures 5a and 5b. During January, maximum cloudiness is observed to occur over the cyclonically-active regions of the north Atlantic, north Pacific, and sub-Antarctic oceans; over equatorial Brazil, Africa, and Indonesia; and over the Barents Sea and northwestern Europe. Minima are found over the continental deserts of Asia, Africa, Australia, and North and South America; over eastern Siberia, and over the sub-tropical oceans. During July (Figure 5b) the cloud maxima persist over the Atlantic, Pacific, and southern oceans, and there is a slight northward shift of the cloud maxima in the equatorial tropics. The summertime maximum of stratus clouds in the Arctic is clearly evident. The extent of the regions of minimum cloud cover over the deserts has also expanded relative to the January situation.

The GLAS GCM global cloud climatology is shown in Figures 6a and 6b. Here the digital value represents the range of cloud frequency in tenths, e.g., an integer 3 indicates that the cloud frequency lies in the range 30-39%. For emphasis, regions where the convective cloudiness exceeds 30% are enclosed by a solid line, and similarly for regions where the frequency of supersaturation or total cloudiness exceeds 70%.

From figures 6a and 6b it is evident that the GCM reproduces the convective maxima over Brazil, Africa, and Indonesia, and the northward migration of this maxima from January to July. The cyclonically-active regions of the north Atlantic and north Pacific show some slight convective activity, as do the southern oceans. The eastern regions of the subtropical oceans are essentially devoid of convective activity.

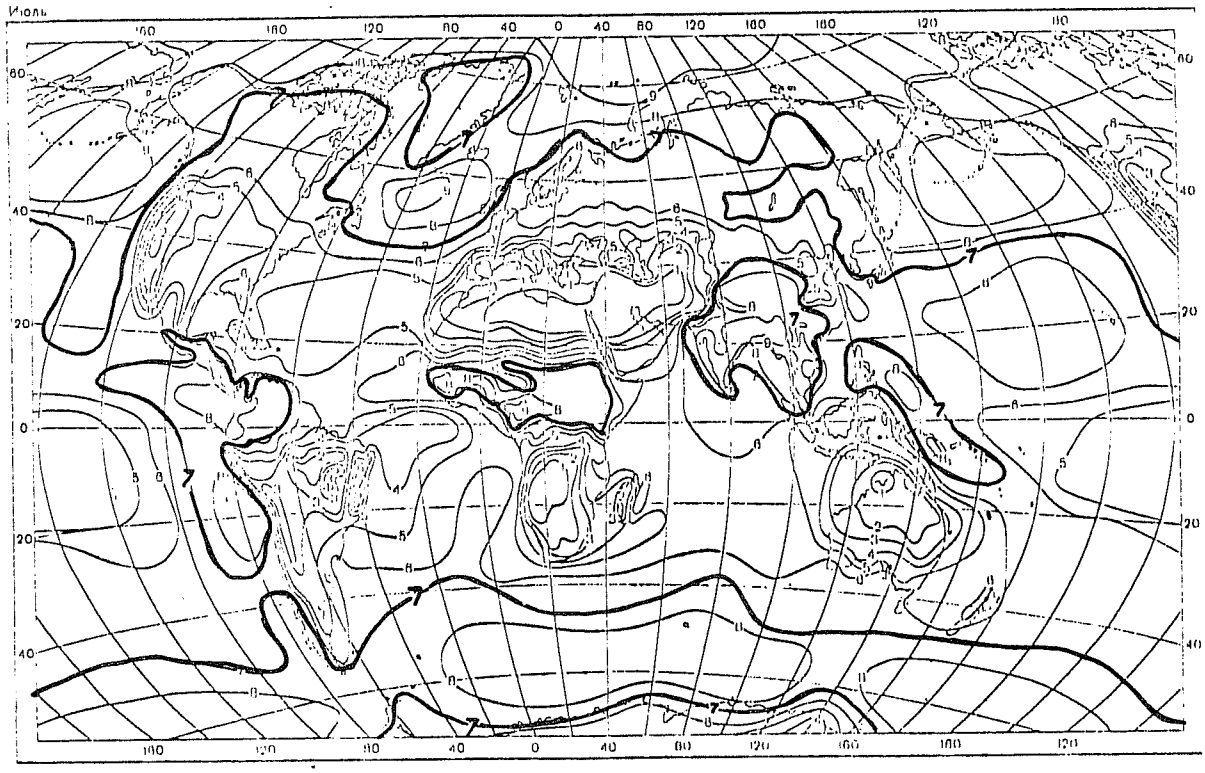

Figure 5a. Observed distribution of cloudiness (January). (After Berlyand and Strokina, 1980).

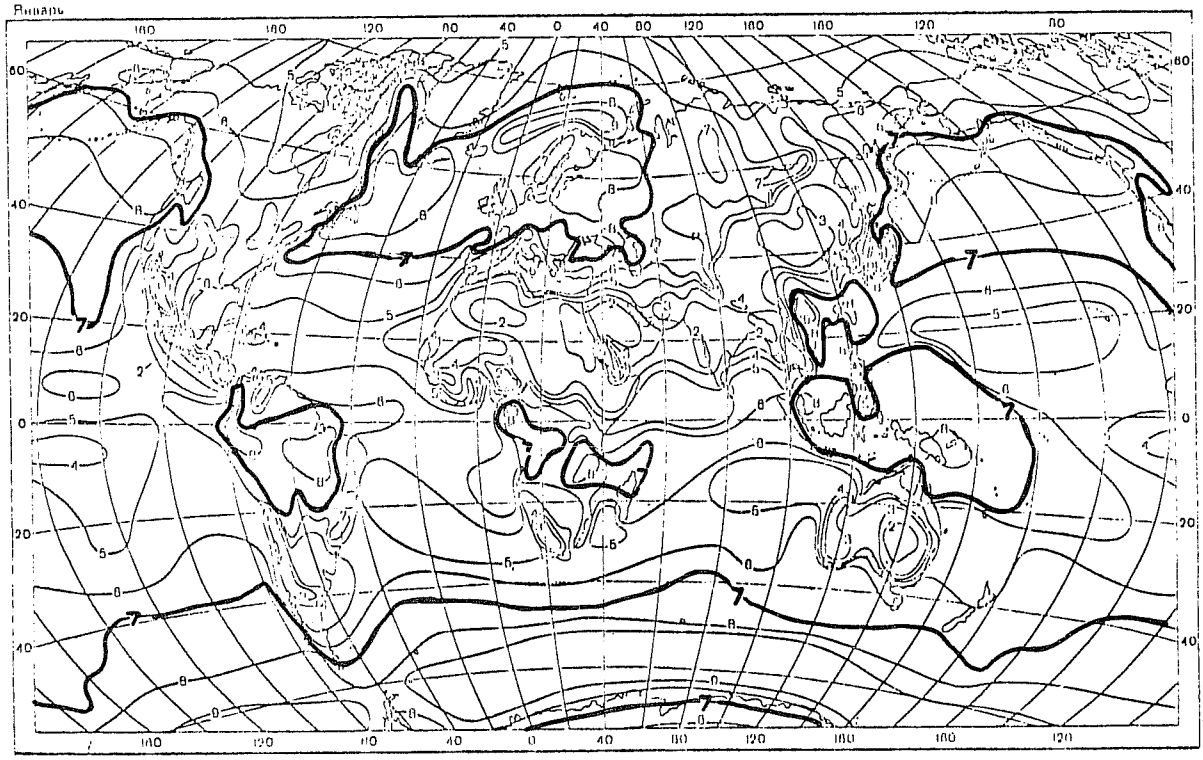

Figure 5b. Observed distribution of cloudiness (July). (After Berlyand and Strokina, 1980).

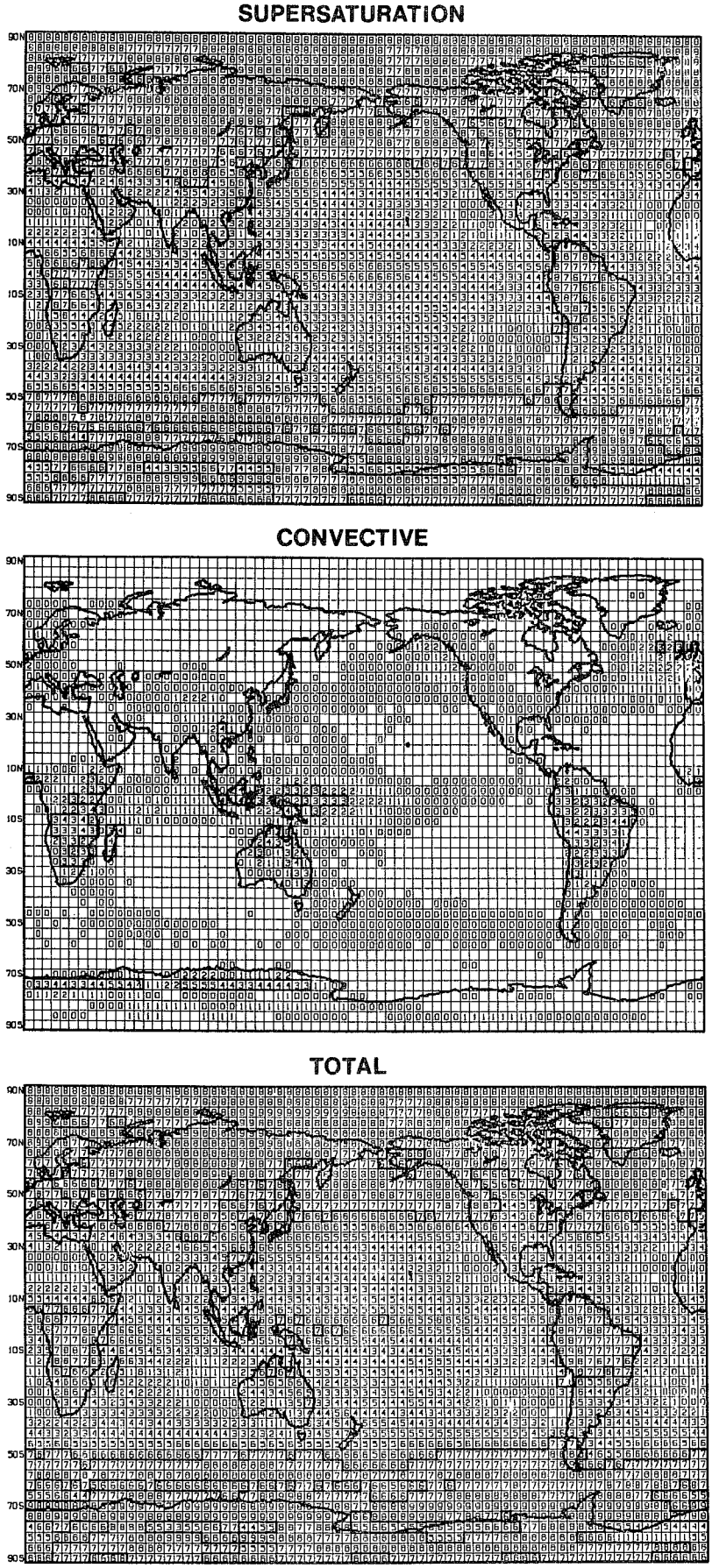


Figure 6a. Digitized cloud frequencies for January.

**SUPERSATURATION**

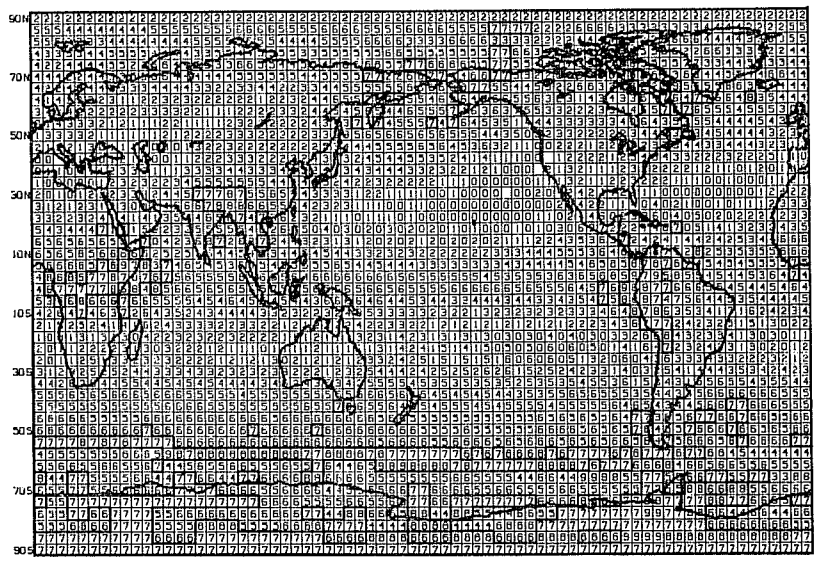

**CONVECTIVE**

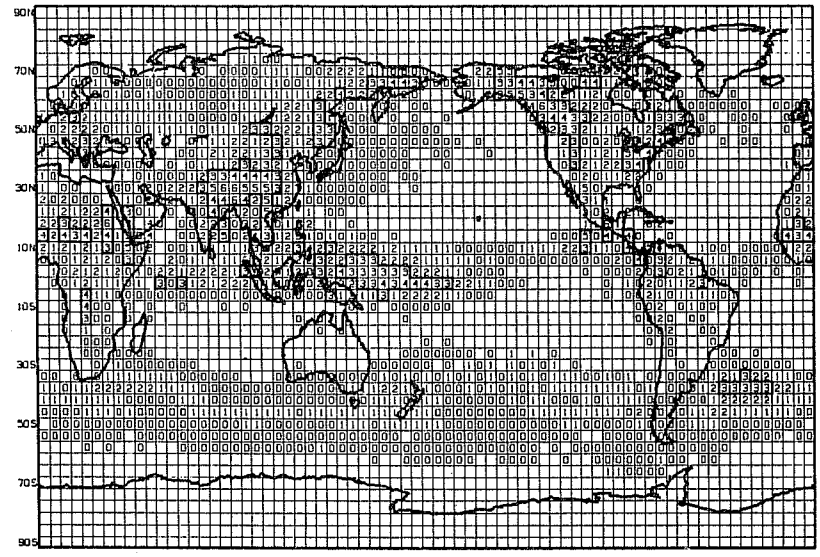

**TOTAL**

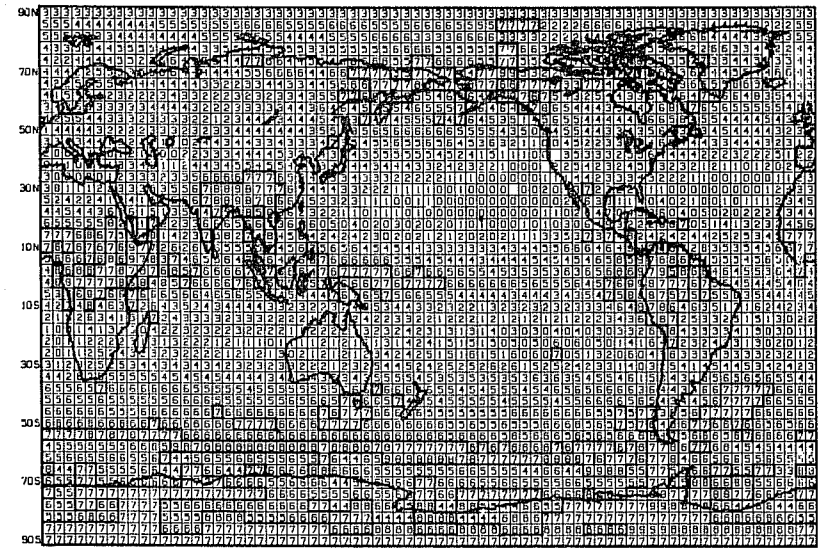

Figure 6b. Same as figure 6a, except for July.

The supersaturation or stratiform cloud cover of the model is also illustrated. The simulated maxima and minima during January generally agree with the observations except for the following cases: Extensive supersaturation cloud covers Antarctica, Greenland, the central Arctic basin, and northwestern Siberia. The tropical maxima and minima seem to be well represented. During July the model fails to produce the summertime stratus cover of the central Arctic, and the desert regions of Africa and North America appear to have too much cloud cover.

## 5. CLOUD-RADIATION FEEDBACK IN GLAS GCM EXPERIMENTS.

### 5.1. Albedo change in semi-arid regions.

One of the first cloud feedback experiments conducted with the model resulted from the desert-albedo experiments of Charney et al., (1977) that employed early versions of the GLAS (then GISS) model. Charney's (1975) original hypothesis for the expansion of deserts involved a positive feedback between large-scale subsidence and the surface albedo, and was independent of cloud formation processes. Stated briefly, it was proposed that increasing the surface reflectivity (through agricultural processes) would decrease the net radiation available to the surface, and would thus enhance large-scale subsidence through the response of a thermally-driven, frictionally-controlled circulation. The subsidence, in turn, would inhibit precipitation and the growth of vegetation, and thus further increase the albedo. This process might be illustrated by the following simplified feedback loop:

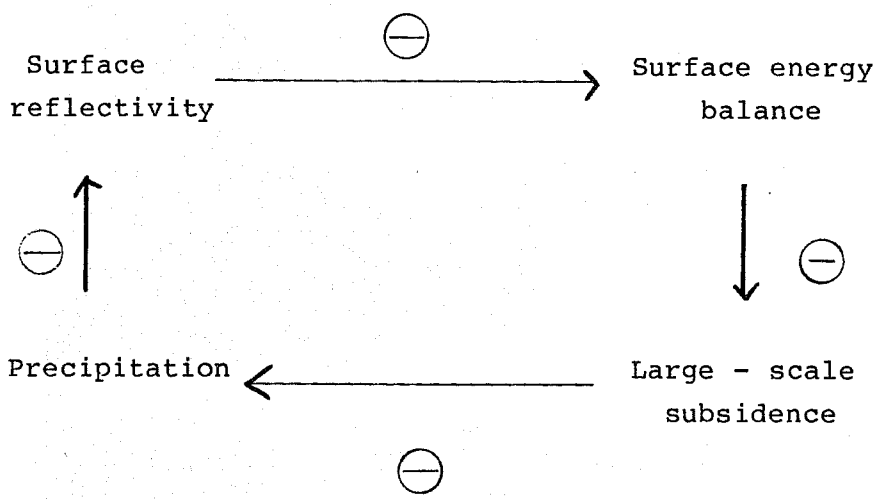

Here a minus (or plus) sign expresses in a schematic way the sense of the correlation between two processes. The feedback of the entire loop would be determined by the product of the signs of the individual links. Thus, the feedback loop shown above would be positive.

The Charney hypothesis was indeed verified in two sets of sensitivity experiments that were conducted with the GLAS GCM. When the albedo in these simulations was increased from 14 to 35% the net radiation at the ground diminished in all of the regions tested, and there was a resultant decrease in precipitation in two of the three regions. However, the cloud formation was handled differently in each of the two sets of experiments, and thus the mechanisms through precipitation was diminished were also different.

The differences between the two experiments are summarized in Table 3. One experiment is refered to as having no cloud feedback since surface evaporation was artifically suppressed and cloudiness differed by only 1-5% between the control and anomaly runs (see Row B). The other experiments were said to have cloud feedback because of the excessive evaporation provided by the parameterizations, and cloud frequency changes ranged between 15-24%.

When no cloud feedback was permitted, the radiation balance decreased by about 46 $Wm^{-2}$, and so did precipitation in most regions, in agreement with the Charney hypothesis. The differences, however, were due almost exclusively to the differences in the absorbed solar radiation caused by the albedo changes. With cloud feedback, the radiation balance also decreased in response to the brighter albedo, but the decrease was not generally due to diminished solar absorption. Rather, it was due to the fact that the infrared balance at the surface became smaller (more negative) due to the suppression of cloud formation. In fact, in two cases (see Row A) the solar radiation at the surface increased slightly because the planetary albedo diminished with the smaller cloud frequencies. Here, too, the precipitation also diminished.

These results illustrate the complicated way in which the cloud effect on the net radiation is linked to the surface brightness.

Table 3. Summary of Changes in Desert Albedo Experiments

| | Control (low albedo) | | | | Differences (high albedo minus control) | | | |
|---|---|---|---|---|---|---|---|---|
| A. Radiation Budget ($Wm^{-2}$) | Feedback | | No Feedback | | Feedback | | No Feedback | |
| | Solar | IR | Solar | IR | Solar | IR | Solar | IR |
| 1. SHL | 172 | -59 | 263 | -141 | 8 | -26 | -47 | 0 |
| 2. RPT | 183 | -48 | 273 | -136 | 9 | -28 | -51 | 5 |
| 3. GP | 189 | -63 | 308 | -176 | -1 | -18 | -59 | 13 |
| B. Cloud frequency (%) | Feedback | | No Feedback | | Feedback | | No Feedback | |
| 1. SHL | 70 | | 40 | | 24 | | 5 | |
| 2. RPT | 77 | | 43 | | 20 | | 1 | |
| 3. GP | 67 | | 21 | | 15 | | 1 | |
| C. Hydrologic Cycle ($Wm^{-2}$) | Feedback | | No Feedback | | Feedback | | No Feedback | |
| | Evap | Precip | Evap | Precip | Evap | Precip | Evap | Precip |
| 1. SHL | 107 | 215 | 4 | 116 | -26 | -99 | 6 | -38 |
| 2. RPT | 119 | 142 | 3 | 61 | -15 | -75 | 5 | 9 |
| 3. GP | 122 | 107 | 0 | 23 | -29 | -43 | 3 | -11 |

D. Cloud Effects on the Radiation Balance ($Wm^{-2}$)

| | Low Albedo | | | High Albedo | | |
|---|---|---|---|---|---|---|
| | IR | Solar | Net | IR | Solar | Net |
| 1. SHL | 82 | -91 | -9 | 56 | -36 | +20 |
| 2. RPT | 88 | -90 | -2 | 55 | -30 | +25 |
| 3. GP | 110 | -119 | -9 | 82 | -61 | +21 |

Regions: SHL-Sahel; RPT-Rajputana; GP-Western Great Plains

Row D of Table 3 shows the effects of cloud feedback. These are the IR balance without feedback minus that with feedback, and the solar balance minus that without feedback, for each of the two surface albedo conditions. Thus in the Sahel, for example, when the albedo was 14%, and the inclusion of feedback increased cloud frequency from 40 to 70%, the infrared balance increased by 82 $Wm^{-2}$, while solar absorption decreased by 91 $Wm^{-2}$, resulting in a net decrease of 9 $Wm^{-2}$. However, over the bright 35% albedo surface, the solar absorption was diminished by only 36 $Wm^{-2}$, because of the smaller differences between cloud and surface albedo. The net cloud effect was thus an increase of 20 $Wm^{-2}$, since the gain in the infrared was 56 $Wm^{-2}$. The surface albedo changes evidently accompany a change of sign in the net cloud effect.

b. Transparent cloud experiments

i. Radiation of balance studies.

A set of experiments was conducted with the GCM to examine further the separate roles that the visible and infrared opacity of clouds plays in determining the radiation balance at the top of the atmosphere. The details of these experiments are described in Herman et al. (1980).

Clouds are frequently said to exhibit an albedo effect when their formation causes the radiation balance to decrease because of their reflection of solar radiation, and a greenhouse effect when the balance is increased by their absorption and re-emission of infrared radiation. The relative roles of the greenhouse and albedo effects were examined in experiments in which the clouds were made transparent to the streams of solar and infared radiation while all other cloud processes such as formation, latent heat release, precipitation and vertical mixing were realistically computed. The differences between the control and the transparent simulations were then interpreted in terms of greenhouse and albedo effects.

The control and perturbation runs were 30 day integrations spanning the period 1-30 January, and were based on 00 GMT 1 January 1975 initial conditions from NMC. Ocean surface temperatures, surface albedo, and polar sea ice boundaries were prescribed, but were allowed to vary climatologically during the simulation.

The globally and hemispherically-averaged results are cited in Herman et al. (1980). In Figures 7 through 9 we illustrate the zonally-averaged values of the net longwave radiation at the top of the atmosphere, the solar radiation absorbed by the earth-atmosphere system, and the net radiation for the control and for the transparent simulations. The role of model-generated cloudiness in limiting the loss of infrared radiation is apparent from the curves for the control and the thermally transparent case: Without a greenhouse effect the radiation balance would become more negative at all latitudes, with the largest differences occurring in the tropics and in the warmer summer hemisphere. On a hemispheric basis, when clouds do not interact with thermal radiation, the radiation lost to space in the Northern Hemisphere, Southern Hemisphere, and globally increases on the average by 29, 40, and 34 $Wm^{-2}$, respectively.

The extent to which clouds increase the planetary albedo and thus decrease the solar radiation available is seen by comparing the curves in Fig. 8 for the solar radiation absorbed by the earth-atmosphere system for the control, with that for the solar transparent case. It is clear that clouds decrease the solar radiation budget at all latitudes, with the differences again being largest in the tropics and in the summer hemisphere. When clouds become transparent to solar radiation, the amount of solar radiation absorbed by the earth-atmosphere system increase on the average in the Northern and Southern Hemispheres, and globally by 34, 97, and 65 $Wm^{-2}$, respectively.

The net cloud effect on the net radiation balance is the combined effect of the greenhouse and albedo mechanisms. Under limited conditiohs it is possible to compute the net effect of the clouds on the radiation balance simply by adding the radiation loss due to the albedo effect and the gain due to the greenhouse effect. This would be possible only if the changes caused by the two processes were indepedent, i.e., only if the role of thermal radiation in cloud formation processes were unrelated to cloud-solar radiative interactions. The two fields of radiation may be coupled in a variety of ways. For example, warming of the ocean mixed layer through the absorption of solar radiation could induce deep cumulus convection, and thus decrease the longwave loss at the top of the atmosphere.

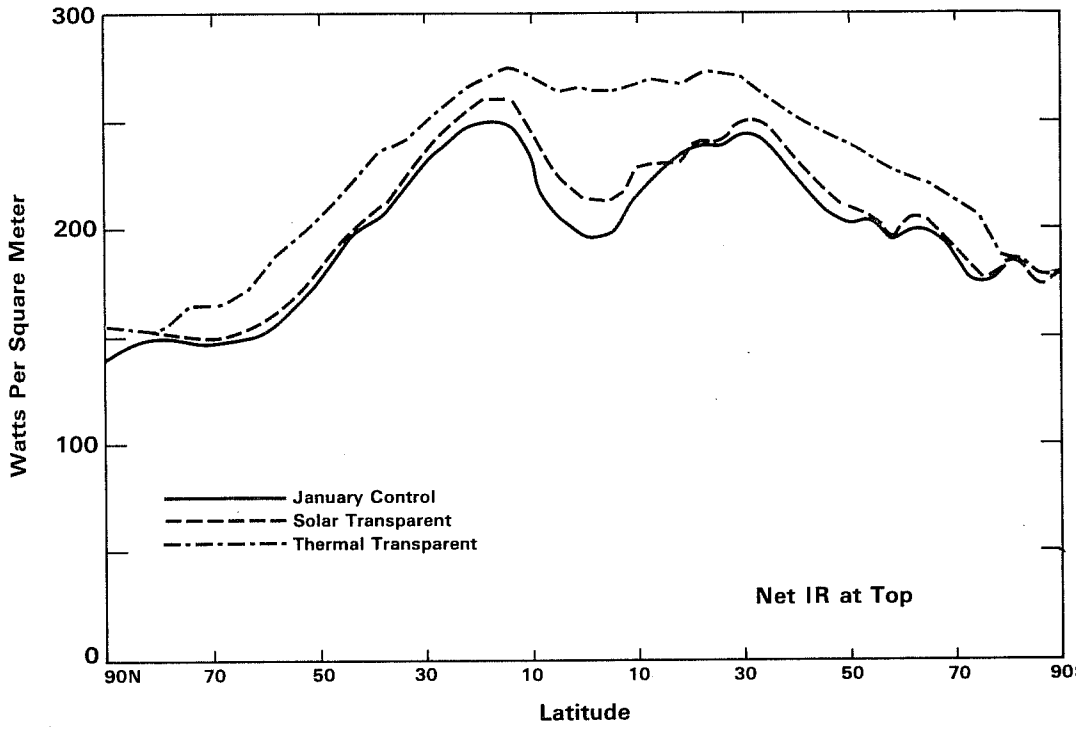


Figure 7. Zonally-averaged longwave radiation at top of atmosphere for control and transparent cloud simulations.

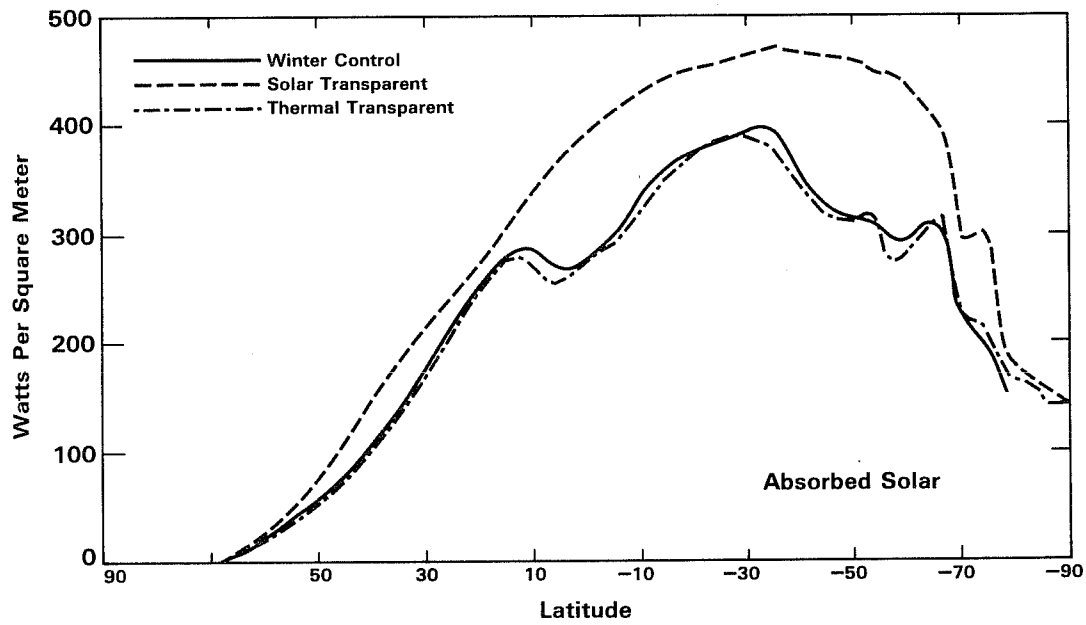


Figure 8. Zonally-averaged shortwave radiation absorbed by earth-atmosphere system for control and transparent cloud simulation.

The zonal distribution of the net cloud effect, $\Delta N$, is shown in Fig 9. In the Northern (winter) Hemisphere the cloud effect is positive, or slightly negative, indicating that the greenhouse effect of clouds dominates their albedo effect, and clouds tend to increase the radiation balance by longwave emission more than they decrease it by reflecting solar radiation to space. In the Southern (summer) Hemisphere the net cloud effect is strongly dominated by the albedo effect. The areally-averaged values are +9 $Wm^{-2}$, -42 $Wm^{-2}$, and -16 $Wm^{-2}$ for the Northern Hemisphere, Southern Hemisphere, and globe, respectively.

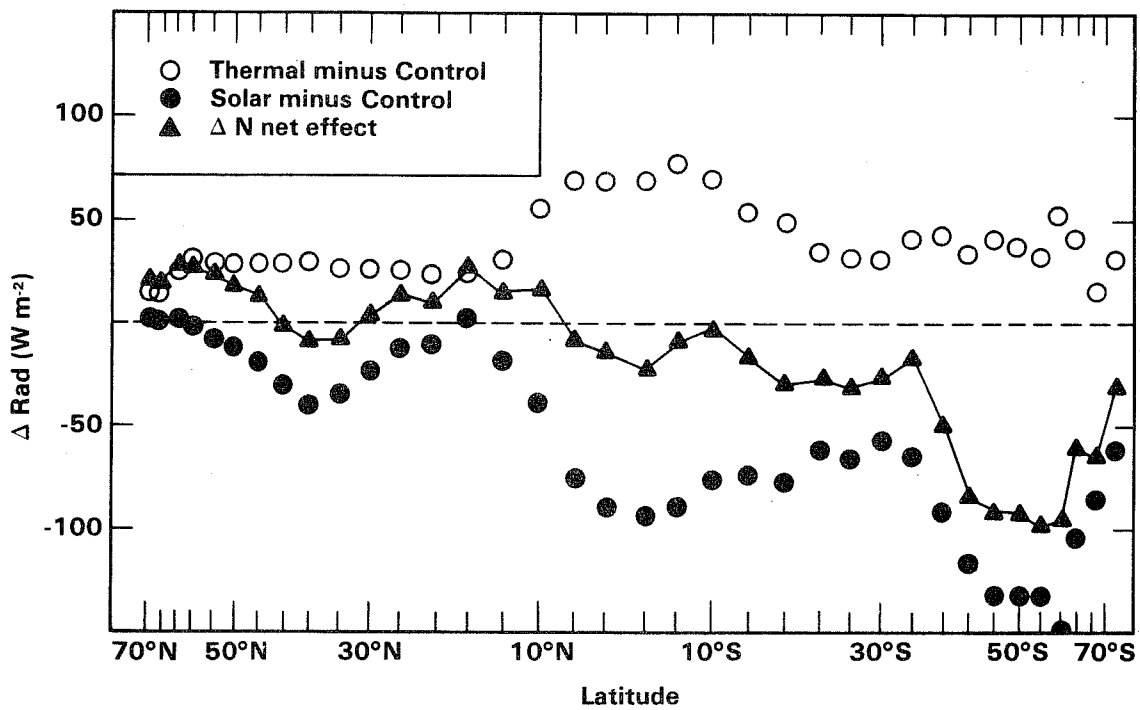


Figure 9. Cloud effect on the net radiation. Open circles are differences between control and clouds which are transparent to thermal radiation; closed circles are differences between control and clouds transparent to solar radiation. Triangles indicate net cloud effect on the net radiation.

Ellis (1978) recently deduced the net cloud effect by computing global radiation budgets from satellite data obtained under clear and cloudy conditions. For the same regions listed above Ellis obtained a net cloud effect of -12 $Wm^{-2}$, -42 $Wm^{-2}$, and -27 $Wm^{-2}$ for the January-February period. These results agree well with the GCM values in the Southern Hemisphere, but conflict with the model results by showing a dominant albedo effect in the Northern Hemisphere. This discrepancy may be another consequence of the

previously discussed problem of unrealistic thermally opaque clouds in the GLAS model.

ii. Cloud-feedback studies

Although the cloud opacity was effectively set to zero in the transparent cloud simulations, clouds were still allowed to exist, and partake in all of the other dynamical functions that the GCM provides. It is thus possible to draw some conclusions about the means through which aspects of the model's dynamics are coupled to solar and infrared radiative processes in clouds. In particular, it is possible to investigate how cloud radiative processes interact or feedback on cloud formation processes.

Sea surface temperatures in the GCM are prescribed, and consequently the formation of convective clouds and supersaturation clouds over water in the GLAS GCM depends only on the response of the atmosphere to the changing radiative conditions. The increase (or decrease) of atmospheric temperature relative to the ocean surface due to radiative processes thus suppresses evaporation and sensible heat transfer at the surface and lowers (or raises) the relative humidity at other levels. Similarly, the heating (or cooling) of the water vapor in the lower troposphere would decrease (or increase) vertical stability. A possible feedback loop would be:

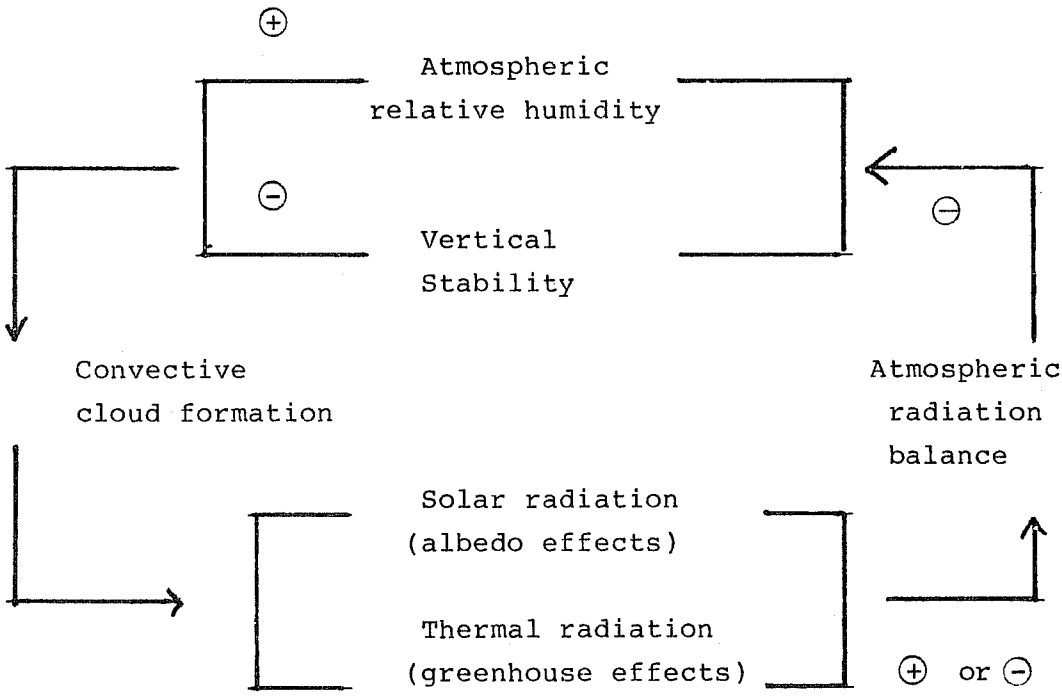

As drawn, the sign of the feedback loop depends on the relative roles of the albedo and greenhouse effects. If the albedo effect dominates,then the loop is positive, and decreasing the radiation balance becomes favorable for further cloud development. The changes in cloud frequency for convective and supersaturation clouds are shown in Figures 10 and 11. The increase in cloud frequency due to albedo effects clearly dominates the decrease due to greenhouse effects for supersaturation clouds. The differences are harder to discern for convective clouds.

Convective clouds over land tend to increase (or decrease) as the net radiation at the surface increases (or decreases) because of the strong dependency of the evaporation and sensible heat exchange on the net radiation at the surface. These clouds in a sense participate in a negative feedback loop since their occurrence causes the surface energy balance to change in a direction that is unfavorable for their further development or maintenance. This interaction can be summarized by the following feedback loop.

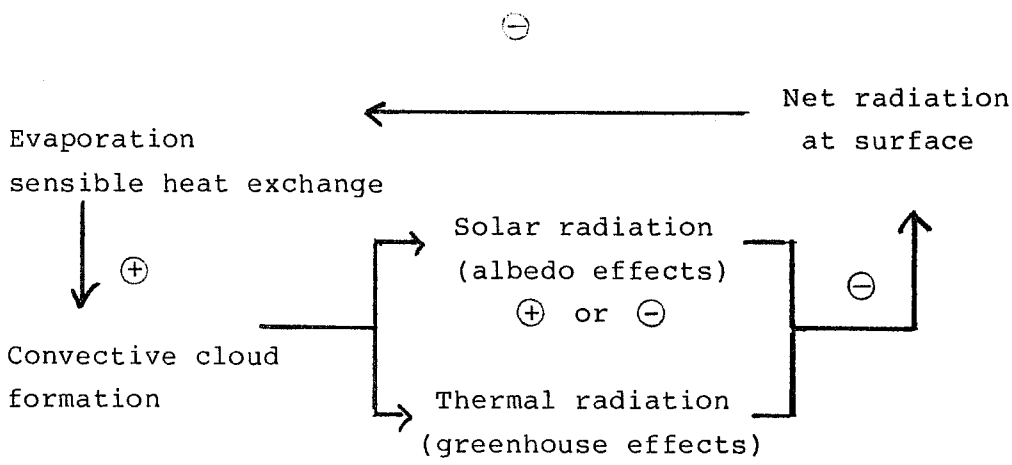


As drawn, the sense of the complete feedback loop again depends on the relative influence of the albedo and greenhouse effects on the surface radiation balance. Here we have assumed that the albedo effect dominates. This behavior is illustrated in Fig. 12, although there is much scatter to the data.

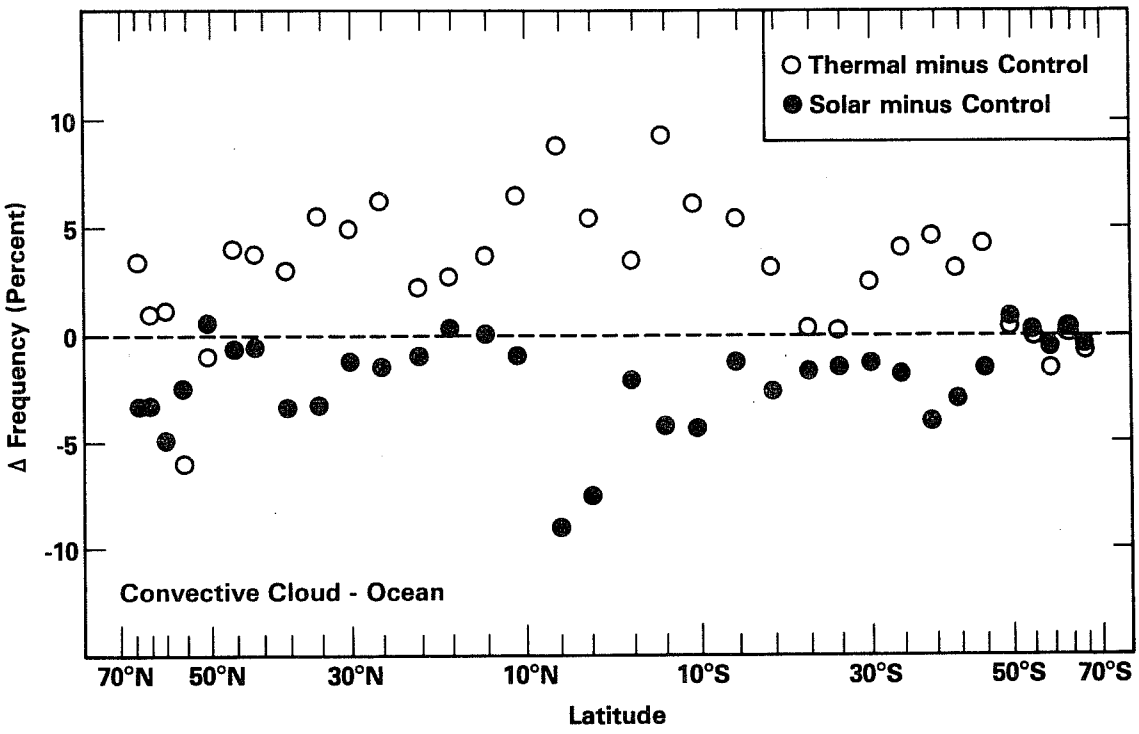


Figure 10. Differences in convective cloud frequency over water for control and transparent simulation.

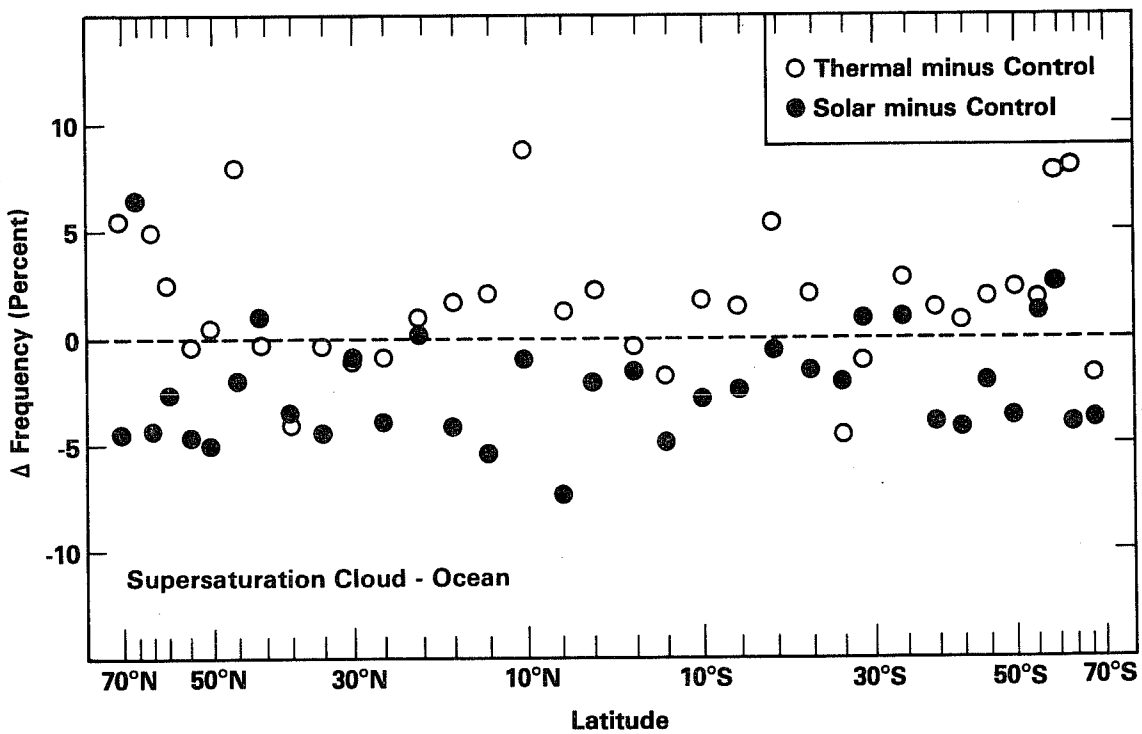


Figure 11. Same as Figure 10, except for supersaturation cloud.

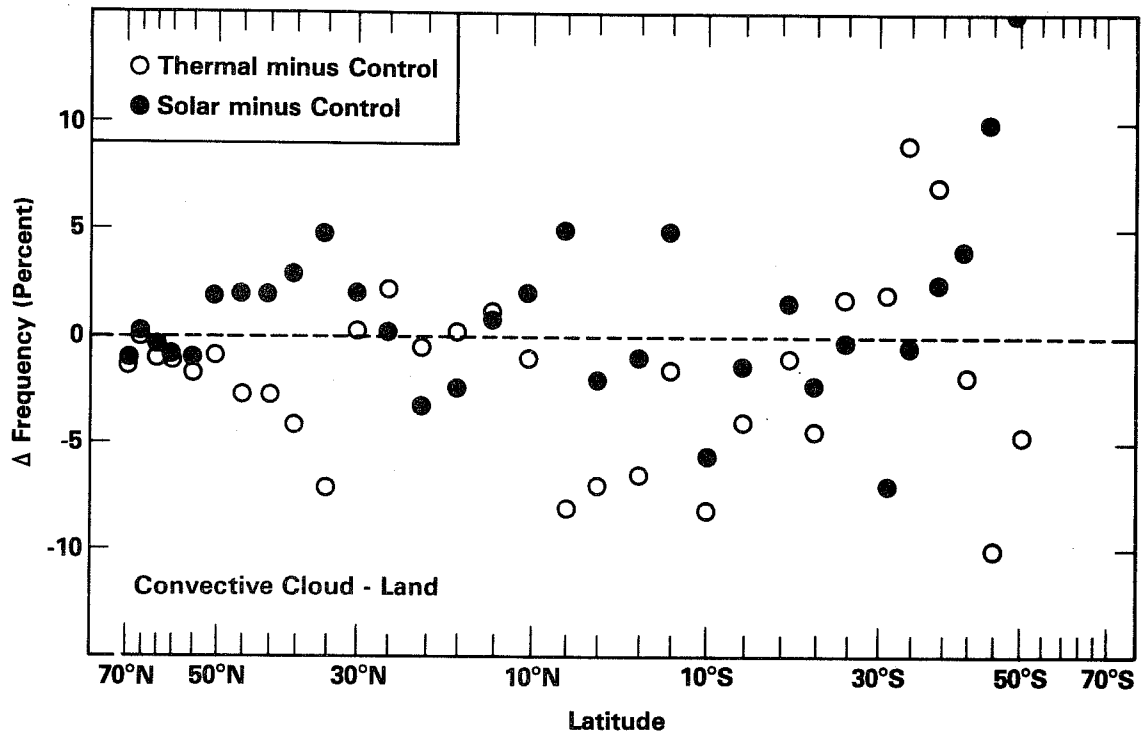


Figure 12. Same as Figure 10, except over land.

c. Fixed clouds vs. variable clouds.

It has sometimes been suggested (e.g., Hunt, 1978) that the general circulation may be adequately modelled with cloud fields that are specified according to a predetermined climatology, and which do not change or adjust their distribution to be consistent with other aspects of the model's dynamics. Some of the consequences of constraining the global cloud distribution to remain invariant were were demonstrated in GCM experiments (see Shukla and Sud, 1980) conducted with variable cloud fields produced by the GCM, and compared with those based on stationary, pre-computed cloud fields. The largest differences in cloud distribution generally occured in the tropical and subtropical regions, where fixed loci of convective clouds replaced the nearly-randomly occurring convective clouds of the GCM. One major consequence of the fixed cloud distribution was that stationary sources and sinks of radiative energy were introduced in low latitudes, replacing the smoother distribution that resulted from the variable occurrence of clouds. These differences were largest in the tropical western Pacific, and in

the peripheral Antarctic oceans, where the monthly-averaged fixed cloud frequencies were 10-20% greater than in the control. Relatively large differences were obtained between the low-latitude hydrologic cycle of the two runs. The zonally-averaged evaporation in the variable cloud control was significantly greater than in the fixed cloud run. (see Figure 13)

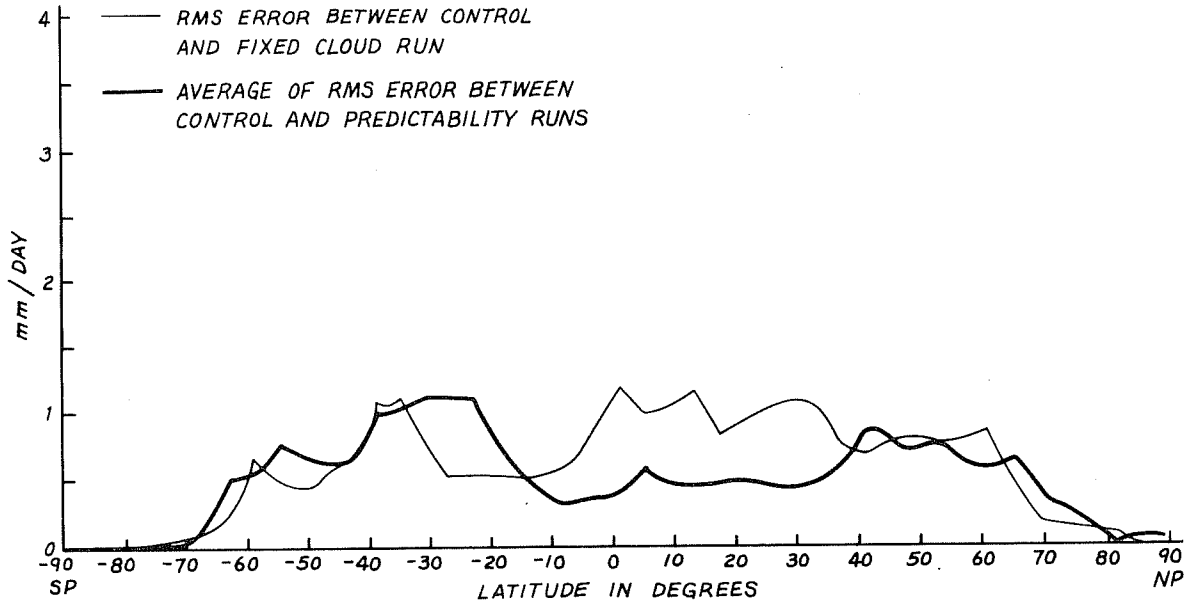


Figure 13. Difference in evaporation rate between fixed and variable cloud experiments, and differences in evaporation caused by random perturbations of initial conditions.

This result is easy to understand in view of the discussion in Section 5b. Since cloudiness over the oceans was greater in the fixed cloud run, low level atmospheric temperatures increased through greenhouse-type mechanisms, and evaporation was suppressed since the prescribed ocean surface temperatures could not respond to the changing cloud conditions. In mid-and high latitudes the differences were insignificant as compared with the inherent variability of the model.

It has thus far proved difficult to isolate the differences between specific meterological features in the fixed and variable cloud runs. One difference however, is easy to deduce: The generation of eddy available potential energy (EAPE) depends upon the correlation of diabatic heating and temperature around a latitude circle, and its storage upon the variance of temperature. To the extent that the localized heat source effect of the fixed clouds increases

temperature differences around latitude circles, EAPE will be increased. This behavior is, in fact, borne out in the model results for the Northern Hemisphere (see Table 4). The changes in the other terms in the energy cycle are generally insignificant.

Table 4

N. HEMISPHERE

**ENERGY CYCLE**

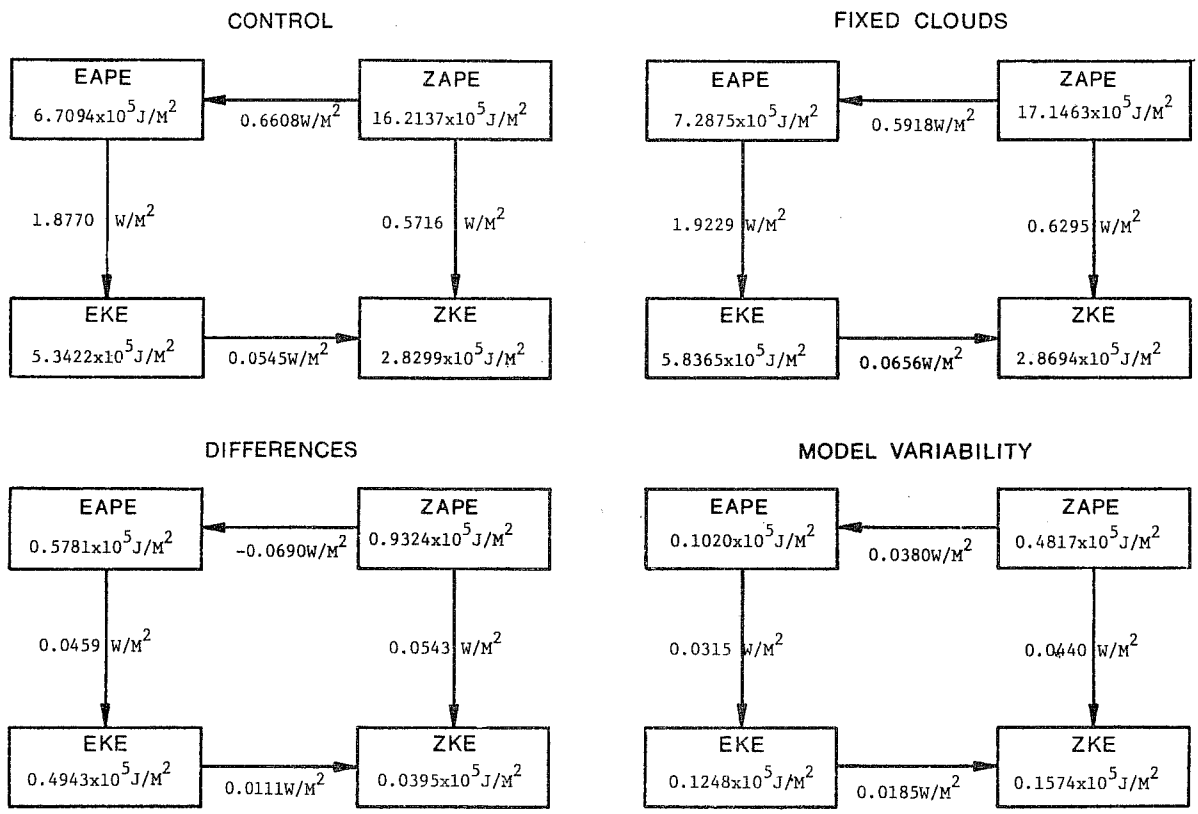


d. Dynamics of the Siberian High.

A chronic deficiency of many major GCM's, including the GLAS model, has been the inability to simulate accurately either the breadth or the intensity of the wintertime Asiatic high pressure regime. The Siberian high in nature is extensive, and covers a broad region of the Soviet Union from the Caspian Sea to northeastern Siberia. Mean monthly sea level pressures in the core of the anticyclone exceed 1032 mb, while daily station reports frequently exceed 1060 mb (Lydolf, 1977). The winterime Siberian high has been poorly

developed in recent versions of the GLAS GCM, with maximum sea level pressures of 1024 mb confined to a small region of northeast Siberia.

In view of the unrealistically high frequency of supersaturation clouds produced by the GCM over Siberia, and the resultant error that this feature has introduced into the model's radiation balance (see Section 4), it was reasonable to suspect that the failure of the high to develop may be due to a radiative mechanism.

A salient characteristic of the Siberian region is its extremely large radiative deficit at the surface and at the top of the atmosphere during the winter. The Siberian anticyclone owes its existence to this deficit in a number of ways: first, by maintaining local surface temperatures that are significantly colder than those in any of the surrounding regions (e.g., the central Arctic, Tibetian plateau, western USSR, or Sea of Okhotsk), a direct thermal circulation is established which results in large-scale subsidence and low-level divergence. Thus, through a mechanism analogous to that in Charney's desert-albedo feedback theory, a radiative deficit at the surface sustains itself by generating anticyclonic vorticity and inhibiting cloud formation. At the same time the extremely cold ground temperatures stabilize the planetary boundary layer, and minimize the turbulent exchange of momentum, heat, and moisture. Thus, convection and evaporation are suppressed, and, as postulated by Y. Mintz, so is frictional convergence and the generation of cyclonic vorticity through Ekman pumping mechanisms.

A possible way of illustrating these mechanisms might be:

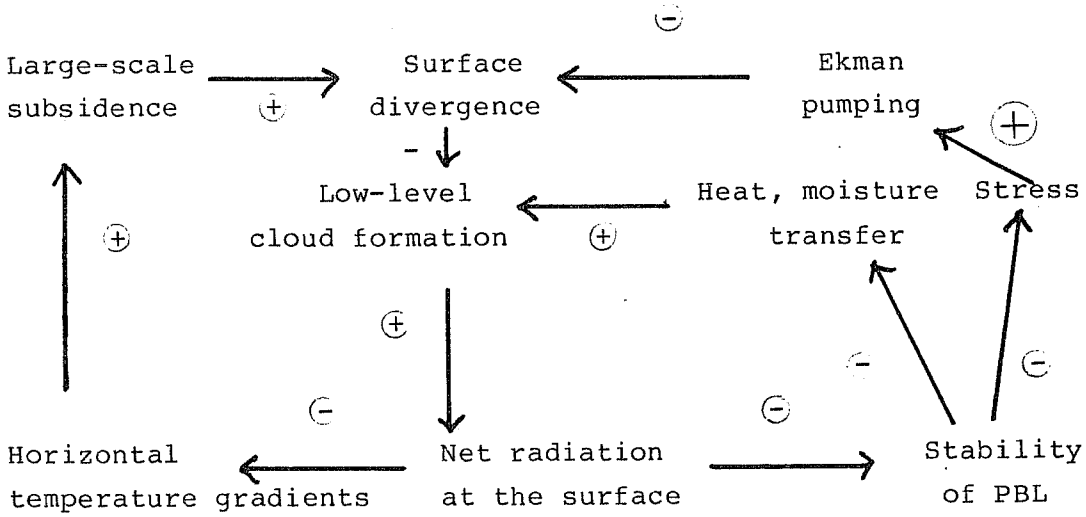

All of the feedback loops shown are stable, and suggest that the Siberian high is a self-perpetuating phenomena, mainly through the modes by which the radiative deficit at the surface limits low-level cloud formation, and perpetuates the excessive infrared loss.

It is thus possible to understand the GCM's problems over Siberia: If the clouds that form in the model are more opaque and more extensive than those in nature, then the surface radiation budget will be enhanced through the greenhouse effect, and anticyclogenesis will be inhibited. Similarly, if the PBL parameterization does not provide a sufficient damping of turbulence under stable conditions, then the generation of cyclonic vorticity will be favored, as will the heat and water vapor transfers. (We have, of course, excluded advection from this discussion, together with the influence of topography and finite differencing schemes on the cylonic vorticity advected into the Siberian region. Differences between sea level pressure reduction techniques used in the GCM and in the observations may also play a role).

The role of longwave radiation in the development of the high is clearly evident from the results of the transparent cloud experiments. In the control (Fig.14) only a weak region of high pressure forms near the Arctic coast, and low pressure from eastern Europe expands throughout Central Asia. In the simulation in which the model's clouds are transparent to thermal radiation, (Fig.15) the Siberian high is extensive and well-developed.

## 6. SUMMARY AND CONCLUSIONS

There are several implications regarding the problems of cloud effects and cloud feedback that follow from the results presented here.

First, the disposition of longwave radiation in this version of the GLAS model is unrealistic, and this is due principally to the problems of treating cloud fraction and variable cloud emissivity. The problem of determining a realistic distribution of cloudiness on the sub-grid scale clearly is substantial. At present it is not possible to prescribe the fractional distribution of cloudiness since there has been no comprehensive data based study that provides the distribution of cloud geometry and phase on scales required for

modeling studies. At the same time there is no satisfactory theory yet available for predicting fractional cloudiness from internally-generated model variables, although some encouragement can be drawn from the cumulus parameterizations being developed by Arakawa, Schubert and others.

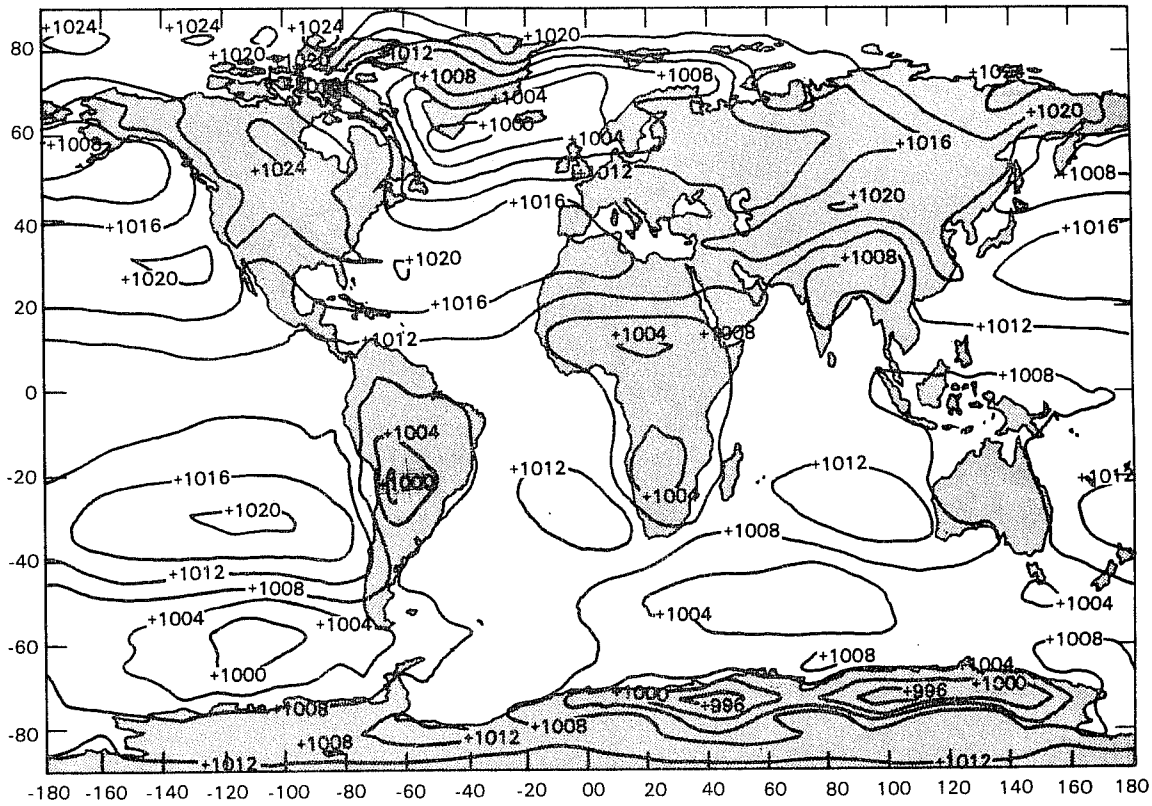


Figure 14. Sea level pressure (mb) for winter control.

The disposition of solar radiation is likewise as dependent on cloud fraction, cloud distribution and cloud optical properties. The calculation of solar absorption with currently available radiative transfer models is dependent to a critical degree on difficult-to-measure parameters such as single scatter albedo and particle phase function. It clearly is important that a hierarchy of carefully-controlled GCM experiments be conducted in order to demonstrate the sensitivity of the simulated climate to these uncertain parameters.

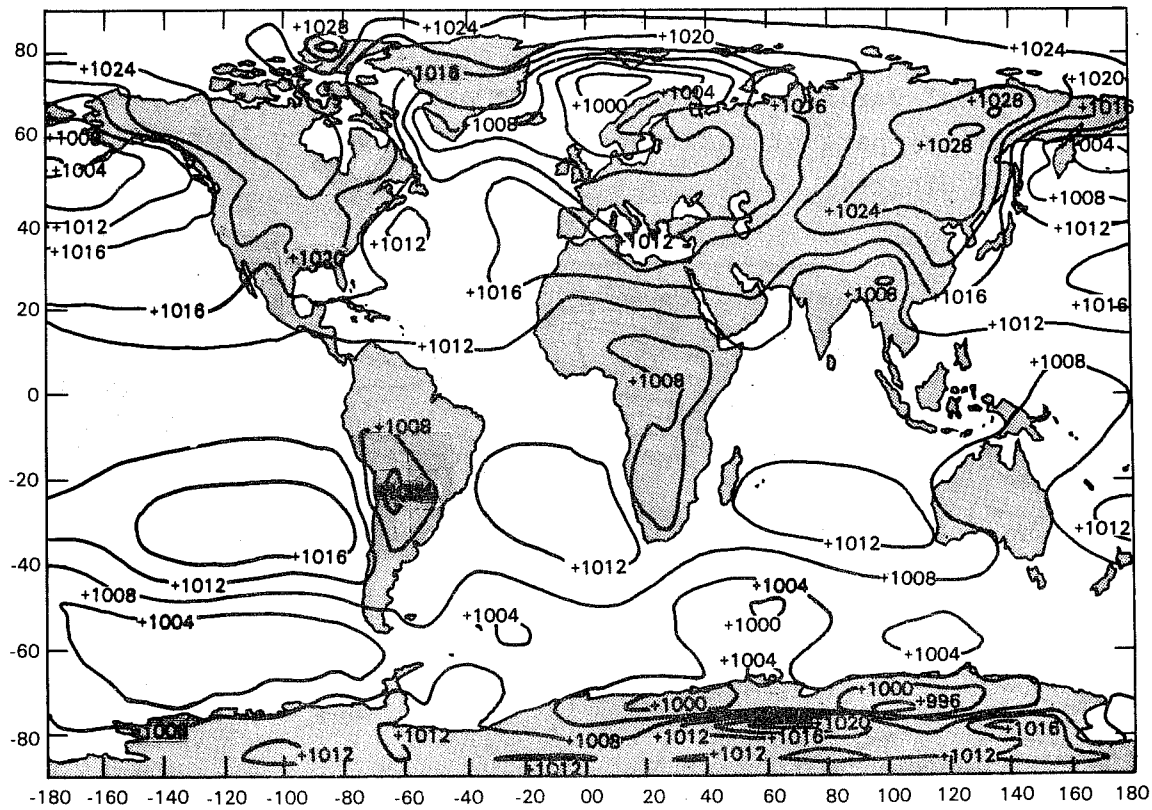


Figure 15. Same as Figure 15, except for clouds transparent to longwave radiation.

Several potential "feedbacks" between cloudiness and the general circulation have been illustrated. The question still remains, however, as to what constitutes a significant feedback. The systematic cloud frequency changes reported here were generally on the order of 5%, and these resulted from very large perturbations of the solar and infrared radiation budgets. While the changes are above the level of inherent model variability, the question still remains as to whether or not the resultant perturbations in the radiation field would result in significant changes in the atmospheric circulation. Some local features, such as the development of the Siberian high, clearly depend on the proper simulation of cloud feedback processes. On the other hand, Wetherald and Manabe (1980) suggest that the result of variable solar constant experiments were essentially independent of cloud feedback in the model. Clearly, a variety of well-planned GCM experiments needs to be conducted to elucidate these questions further.

## 7. ACKNOWLEDGEMENTS.

I am indebted to Dr. Halem and and the Staff of the GLAS Modeling and Simulation Facility for providing the support and resources for these analyses. Discussion with Drs. Y. Mintz, E. Kalnay-Rivas, and J. Shukla are gratefully acknowledged. Programming support was provided by W. Johnson and C. Long. Support for this research was provided by NASA grant NSG-5152 to the University of Wisconsin.

References

Berlyand, T. G. and L. A. Strokina, 1975: Seasonal cycle of tropospheric cloudiness, Trans. Voekova, Main Geophy. Obs., 338.

Berlyand, T. G. and L. A. Strokina, 1980: Global Distribution of a Cumulative Number of Clouds. Leningrad: Gidrometeoizdat.

Charney, J. G., and W. J. Quirk, S. H. Chow, and J. Kornfield, 1977: A comparative study of the effects of albedo change on drought in semiarid regions. J. Atmos. Sci., 34, 1366-1385.

Charney, J. G., 1975: Dynamics of deserts and droughts in the Sahel. Quart, J. R. Met. Soc., 101, 193-202.

Davies, R., 1980: Absorption of solar radiation in a general circulation model: The effect of solar zenith angle. Preprint Volume. Atm. Rad. Symp., Fort Collins.

Ellis, J. S., 1978: Cloudiness, the planetary radiation budget, and climate. Ph.D. Thesis, Colorado State University 129 pp.

Gates, W. L. and M. E. Schlesinger, 1977: Numerical simulation of the January and July global climate with a two-level atmospheric model. J. Atmos. Sci., 34, 36-76.

Halem, M., J. Shukla, Y. Mintz, M. L. Wu, R. Godbole, G. Herman, and Y. Sud, 1979: Comparison of observed seasonal climate features with a winter and summer numerical simulation produced with the GLAS general circulation model. World Meteorological Organization, GARP Publication Series, No. 22 pp 207-253.

Helfand, H. M., 1979: The effect of cumulus friction on the simulation of the January Hadley circulation by the GLAS model of the general circulation. J. Atmos. Sci., 36, 1827-1843.

Herman, G. F. and W. T. Johnson, 1978: The sensitivity of the general circulation to Arctic sea ice boundaries. Mon. Wea. Rev., 106, 1649-1664.

Herman, G. F., M. L. Wu, and W. T. Johnson 1980: The effect of clouds on the earth's solar and infrared radiation budgets. J. Atmos. Sci., 37, 1251-1261.

Herman, G. F. and V. Krishnamurthy, 1981: Fractional cloudiness and variable cloud emissivity in the GLAS GCM. NASA GLAS Modeling and Simulation Facility, Annual Review.

Herman, G. F. and W. T. Johnson, 1980: Arctic and Antarctic climatology of the GLAS GCM. Monthly Weather Rev., 108, pp. 1974-1991.

Hunt, G. E., 1978: On the general circulation of the atmosphere without clouds. Quart, J. R. Met. Soc., 104, 91-102.

Lacis, A. A. and J. E. Hansen, 1974: A parameterization for the absorption of solar radiation in the earth's atmosphere. J. Atmos. Sci., 31, 118-133.

Lydolph, P. E., 1977: Climates of the Soviet Union. In: World Survey of Climatology, Vol. 7. New York: Elsevier, 443 pp.

Rodgers, C. D. and C. D. Walshaw, 1966: The computation of infrared cooling rate in planetary atmospheres. Quart J.R. Met. Soc., 92, 67-92.

Shukla, J. and V. Bangaru, 1979: Effect of a Pacific sea surface temperature anomaly on the circulation over North America: A numerical experiment with the GLAS model. WMO GARP Publication Series, 22, 501-518.

Shukla, J. and Y. Sud, 1980: Effect of cloud-radiation feedback on the climate of a general circulation model. Manuscript submitted to J. Atmos. Sci.

Somerville, R. C. J., P. H. Stone, M. Halem, J. E. Hansen, J. S. Hogan, L. M. Druyan, G. Russell, A. A. Lacis, W. J. Quirk, and J. Tennebaum, 1974: The GISS model of the global atmosphere. J. Atmos. Sci., 31, 84-117.

Stone, P. H., S. Chow, and W. J. Quirk, 1977: The July climate and a comparison of the January and July climates simulated by the GISS general circulation model. Mon. Wea. Rev., 105, 170-194.

Wetherald, R. T., and S. Manabe, 1980: Cloud cover and climate sensitivity J. Atmos. Sci., 37, 1485-1510.

Winston, J. S., A. Gruber, T. I. Gray, M. S. Varnadore, C. L. Earnest, L. P. Mannello, 1979: Earth-atmosphere radiation budget analyses derived from NOAA satellite data, June 1974-February, 1978. U. S. Dept. of Commerce, National Oceanic and Atmospheric Administration. Vols. I and II.

Wu, M. L., L. D. Kaplan, and R. Godbole, 1978: Influence of systematic radiation differences on the dynamics of a model atmosphere. Preprint Volume, Third Conf. on Atmospheric Radiation, Davis CA. pp. 293-302.

Wu, M. L., 1980: The exchange of infrared radiative energy in the troposphere. J. Geophys. Res., 85, 4084-4090.

Yamamoto, G., 1962: Direct absorption of solar radiation by atmospheric water vapor, carbon dioxide, and molecular oxygen. J. Atmos. Sci., 19, 182-188.